

Article

# Geochemical Signatures of Paleoclimate Changes in the Sediment Cores from the Gloria and Snorri Drifts (Northwest Atlantic) over the Holocene-Mid Pleistocene

Liudmila L. Demina <sup>\*</sup> , Ekaterina A. Novichkova , Alexander P. Lisitzin and Nina V. Kozina

Shirshov Institute of Oceanology, Russian Academy of Sciences (RAS), 117997 Moscow, Russia; enovichkova@mail.ru (E.A.N.); lisitzin@ocean.ru (A.P.L.); kozina\_nina@bk.ru (N.V.K.)

\* Correspondence: l\_demina@mail.ru; Tel.: +7-963-608-17-47

Received: 22 August 2019; Accepted: 3 October 2019; Published: 5 October 2019



**Abstract:** A multiproxy study of the sediment cores taken from the Snorri Drift, formed under the influence of the Iceland–Scotland bottom contour current, and from the Gloria Drift, located southward Greenland at the boundary of Irminger and Labrador Seas, was performed. This area undergoes a variable mixing of polar waters with the warm North Atlantic current, whose intensity and direction seemed to change dramatically with the alteration of warming and cooling periods during the six marine isotope stages MIS 1–6. The relative age of this core does not exceed 190,000 cal yr BP; the average sedimentation rate was 1.94 and 2.45 cm/kyr in the Gloria and Snorri Drifts core respectively. In both the cores, the sediment records showed the downcore co-variation of ice-rafted debris (IRD); and terrigenous elements, such as Si, Al, Ti, Cr, and Zr, were revealed; their values were clearly higher in the glacial periods (MIS 2, 4, and 6) compared to interglacials (MIS 1, 3, and 5). The downcore rhythmic distributions of these elements, as well as Al/Si, Ti/Al, Fe/Al ratios exhibit an opposite trend with that of  $\delta^{18}\text{O}$  values, biogenic components ( $\text{CaCO}_3$ ,  $\text{BioSiO}_2$ ), and Si/Fe and Mn/Fe ratios.

**Keywords:** geochemical indicators; paleoclimate change; sediment core; Gloria and Snorri contourite drifts; XRF analysis

## 1. Introduction

The North Atlantic is one of the key regions of the World Ocean characterized by the global thermohaline circulations interrelated with climate changes [1,2]. An active penetration of relatively warm and saline Atlantic waters to the Arctic Ocean during interglacial periods and deglaciation results in the heating of surface water and their transfer to higher latitudes that leads to intensification of the global ocean conveyor and melting of Arctic ice [3–5]. Sediments are supplied to the pelagic formation by ice- and iceberg-rafting from above and by turbid and contour flows along the seafloor [6].

The contourite drifts were discovered about 50 years ago [7]. They are defined as sedimentary bodies formed under the influence of the system of the along-slope near-bottom currents, so contourite drifts are usually investigated to reconstruct near-bottom paleocurrents speed [8–11]. In the North Atlantic, the contourite drifts have been formed due to the inflow of deep Arctic waters with bottom currents, the speed of which was increased during warming and decreased during glaciation [12–15]. During the Last Glacial Maximum, the Central North Atlantic Gyre served as the major transport belt of icebergs to the North Atlantic [14,16]. The melting ice provided the freshwater input influencing the climate change during the last glacial via the slowing effect of the Atlantic Meridional Overturning Circulation (AMOC) which led to global heat distribution [17].

Intense advection of warm North Atlantic water into high latitudes causes a sharp increase in water productivity [18]. Strong bottom currents influence the lithological characteristics of sediment sequences [19], which can be connected to changes in the past climate. In the drift's core, maximum current velocity corresponds to massive irregular sandy pockets in the cores, while the decreasing of current velocity is reflected in the predominance of mud-laminated cross-laminated silt, at the same time, bioturbation is generally the dominant feature [9]. From this viewpoint, the contourite drifts are of great interest to reconstruct past ocean conditions due to higher sedimentation rates compared to adjacent deep-sea sediments [10].

In the North Atlantic, based on the modes of measured grain size distributions at the Gloria Drift, two sources of the lithogenic ice-rafted debris (IRD) have been identified: ice rafting and the Northwest Atlantic Mid-Ocean Channel [15,20].

The elemental chemical analysis and element ratios of the sediment cores provide an insight into sources of sedimentary material, bioproductivity, ocean circulation, and other parameters of the sedimentation paleoenvironment, as well as post-sedimentation processes [21]. In the North Atlantic, an active stage of the last glaciation was followed by melting icebergs' freshwater input from the Laurentide Ice Sheet through the Hudson Strait that is reflected in the sediment layers enriched in the (IRD) [22]. These paleoevents, named Heinrich-events, are clearly linked to dramatic climate shifts in the Northern Hemisphere. They were identified in the clastic carbonate cores west of the Svalbard archipelago not only by the IRD profiles, but also by variations in such elemental ratios as Ca/Sr, Zr/Ca,  $C_{org}$ , C/N [23]. In the late Quaternary Arctic sections, the Al/Si, Fe/Ca, Ti/Al, and Zr/Al ratios were applied to estimate the variability of clastic components [24,25]. Manganese, as a redox-sensitive element, was used in the sediments of the Lomonosov Ridge in the Arctic Ocean to determine the conditions of anoxia caused by ice cover [26]. The Mn/Fe ratio serves as a proxy of redox conditions and post-sedimentary changes in bottom sediments, as soon as an anoxia leads to a change in the Mn/Fe ratio and contents of Mn-related and some chalcophile metals in the sedimentary cores [27–30]. The Sr/Ca and Rb/Sr ratios in the biogenic carbonate sediments of the South Atlantic were applied as a geochemical proxy of climatic changes: Glacial periods are characterized by high Sr/Ca values, while interglacials are characterized by lower ones [31].

In this work, we aimed to identify changes in the geochemical characteristics of the sedimentation paleoenvironment at the Gloria and Snorri Contourite Drifts based on geochemical multielemental analysis combined with stable isotope and lithological data. The primary goal was to find a correspondence between the climate fluctuation in the Mid-Pleistocene-Holocene and changes in the sedimentological and geochemical properties of sediments. We have made an attempt to test the applicability of some geochemical proxies to describe the main trends of environmental changes in glacial/interglacial periods in the Northwest Atlantic over the Mid-Pleistocene to Holocene covering about 190 kys.

## 2. Sediment Cores and Regional Hydrography

The sediment cores were collected in the Northwest Atlantic during expeditions of the Shirshov Institute of Oceanology on the R/V "Akademik Mstislav Keldysh" in 2002 and "Akademik Ioffe" in 2015. Here, we focused on the two sediment cores sampled with gravity corer: AMK-4493 recovered from the Gloria Drift (53°31.22 N; 42°45.74 W, 3547 m sea depth) and AI-3378 taken from the Snorri Drift (59°29.977 N; 32°50.533 W, 2192 m depth) (Figure 1).

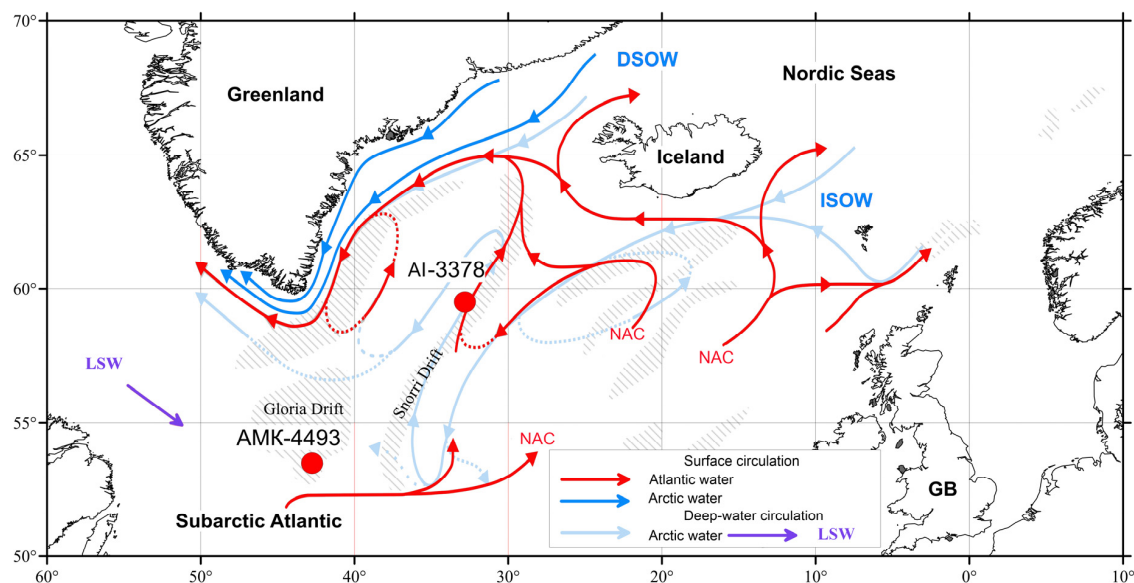


**Figure 1.** Location of sediment sampling stations at the Snorri Drift (AI-3378) and Gloria Drift (AMK-4493) and main surface and deep currents responsible for water exchange between the Atlantic Ocean and Arctic Basin [32]. NAC, North Atlantic Current; IC, Irminger current; EGC, East-Greenland Current; DWBC, Deep Western Boundary Current; DSOW, Denmark Strait Overflow Water; ISOW, Iceland-Scotland Overflow Water; LSW, Labrador Sea Water. Dash shows the position of Gloria and Snorri Drifts.

AMK-4493 core (367 cm core length) was taken from the southeastern part of the Gloria Drift, on the giant sediment waves with a length about 70 m and width up to 2–3 km [15]. The Gloria Drift, located southward Greenland on the boundary of the Irminger and Labrador Seas, is under the influence of the Northwest Atlantic Mid-Ocean Channel (NAMOC), which is a giant submarine drainage system of the Labrador Sea. The sedimentation in the Gloria Drift area was also influenced by the processes of the hemiturbidites formation in the Labrador Sea: IRD was probably transferred there not only by icebergs but was also delivered through the NAMOC [15,33]. Sediments are composed of mainly light brown (with various shades) miopelagic muds (Figure 2). The deposition of IRD-containing hemipelagites, which are rarely interbedded with hemiturbidites, is characteristic of the Gloria Drift. Ice rafted debris of a gravel and pebble size was found throughout the core. Changes in the oxygen isotope data, IRD values and content of  $\text{CaCO}_3$  have shown that the relative age of this core does not exceed 190000 cal BP (the average sedimentation rate is 1.93 cm/kyr).

AI-3378 core (466 cm length) was taken on the eastern flank of the Reykjanes Ridge. This area is influenced by the Iceland–Scotland Overflow Water (ISOW) current [32], which flows southwest along the Reykjanes Ridge. Sediments are presented by the light brown (primary color 10YR/5/3) aleuropelites and are very sandy with a high content of carbonate matter (up to 87%) and traces of bioturbation. There is significant variability in the sand fraction, probably caused by the change in the sedimentary material delivered to the core site. In the 100  $\mu\text{m}$  fraction, carbonate biogenic fossils are predominant. The core is characterized by the alternation of biogenic carbonate layers with the quartz-feldspar ones. The relative age of sediments was determined using the oxygen isotope and  $^{230}\text{Th}$  data, as well as data on changes in IRD and calcium carbonate values, which do not contradict each other and can be considered quite reliable stratigraphic markers. Thus, in the AI-3378 core, six MIS covering no more than 190,000 cal BP (the average sedimentation rate is 2.45 cm/kyr) were identified [34].

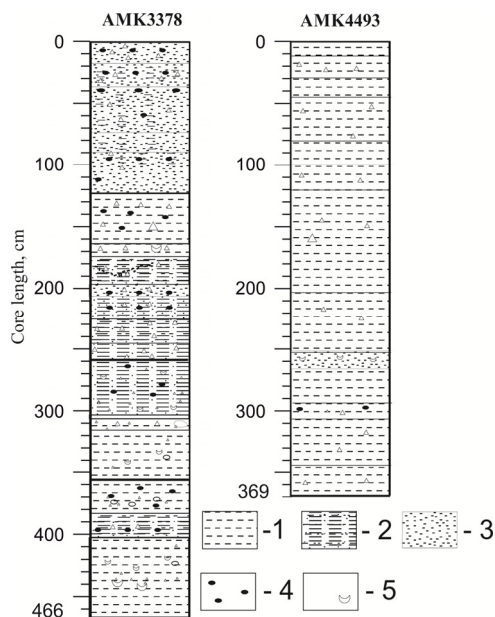


**Figure 2.** Lithology of the Snorri Drift core AMK-3378 and Gloria Drift core AMK-4493. (1) Pelite silt, (2) aleuropelite, (3) sand, (4) hydrotroilite, (5) calcareous detritus.

Both cores were split with intervals of 10 cm for geochemical studies. From our data on sedimentation rates in the areas studied (see above), the 10-cm interval is equivalent approximately to 4–5 ka.

It should be noticed that there are some features of similarity and difference in the cores studied. Both sediment sequences cover six marine isotope stage (MIS). The relatively low sedimentation rates in the cores from the Snorri and Gloria Drifts are related to the average rates in the open Atlantic. It has been established that the average sedimentation rates for pelagites of biogenic (coccolith–foraminifera) origin are about 0.2–4 cm/kyr [35,36]. Both cores are composed of fine-grained material of aleuropelite and pelite grain size fraction. Sand layers, which were more often observed in the AI-3378 core, are mainly related to foraminiferal shells of sand dimension. The difference is that the IRD contents are as much as twice higher in the Snorri Drift core, which is located northward to the Gloria Drift, whereas the IRD maximum reaches 5386 lithic grains/g. However, in the latter, the IRD peaks are more pronounced, and the sand fraction is represented by IRD and foraminiferal tests [15]. In the case of the more northerly core from the Snorri Drift, IRD varied from 258 to 5386 lithic grains/g; in the case of the more southerly core from the Gloria Drift, IRD varied from 0 to 2567 lithic grains/g. [15,20,34,37]. The IRD counts in the northern part (above 55° N) of North Atlantic vary from 6.2 to 4446 lithic grains/g (SU90-24 core, [37]), while in the more southerly area (between 50 and 40° N), the IRD counts vary from <10 to 2212 (AI3646 core, [20]). Therefore, these data generally correspond to the earlier publications [15,20,34,37] and reflect an increase of the IRD abundance northward, i.e. while approximating the glaciers.

### 3. Materials and Methods

#### 3.1. Stable Oxygen Isotope, IRD, TOC, and SiO<sub>2am</sub> Analysis

Stratigraphic subdivision of the AI-3378 and AMK-4493 cores was performed using data on the calcium carbonate, stable oxygen isotope ( $\delta^{18}\text{O}$ ), and IRD records [20,34]. For details, see Table S1 in Supplementary Materials.

Analysis of stable oxygen isotope ratios ( $\delta^{18}\text{O}$ ) in planktonic foraminiferal tests (*Neogloboquadrina pachyderma*  $\geq 30$  specimens, average size  $\sim 150\ \mu\text{m}$ ) was performed by Dr. N. Andersen at the Leinbitz Laboratory of Radiometric Dating and Stable Isotope Research (Kiel University) using a Finnigan MAT 251 mass spectrometer. The accuracy of the method is 0.08‰. Age models for the studied cores are

based on the correlation between our stable planktonic isotope records and standard curve LR04 [38] by means of interpolation between assigned reference points. The IRD data allows us to identify the Heinrich events (H) with the well-known ages [39]; however, due to rather low resolution (commonly 10 cm), not all of them could be identified. There are only two events clearly distinguished in the Gloria Drift core AMK4493: H1 with a time interval of 15,600 and H6 with a time interval of 59,100 cal. yr BP. The three Heinrich events in the AMK3378 core are as follows: H2? (22,400), H3? (26,800), and H6 (57,300) cal. yr BP (Figures 3 and 4). Additionally, an excess  $^{230}\text{Th}$  ( $^{230}\text{Th}_{\text{exc}}$ ) was used as an attempt to estimate the sedimentation rates in the AI-3378 core [34]. In the studied cores, IRD lithic grains were counted in the  $>150\ \mu\text{m}$  fraction using an MBS-10 microscope. Each sample was split using a microsplitter and no less than 300 lithic grains were counted. Samples with low IRD content were fully examined. IRD index was calculated as the number of lithic grains per gram of dry sediment (grains/g). In the AI-3378 core, lithic grains were calculated with a 10-cm step and in the AMK-4493 core, with a 2-cm step [15,34,40]. The total carbon and total organic carbon (TOC) contents were determined by automatic coulometry with an AN 7529 carbon analyzer (precision 0.01%). The contents of  $\text{CaCO}_3$  were calculated from  $C_{\text{carb}}$  with a coefficient of 8.3. The concentration of biogenic amorphous silica ( $\text{SiO}_{2\text{am}}$ ) in the Snorri Drift core was determined by colorimetric method with a precision of 0.05% [41].

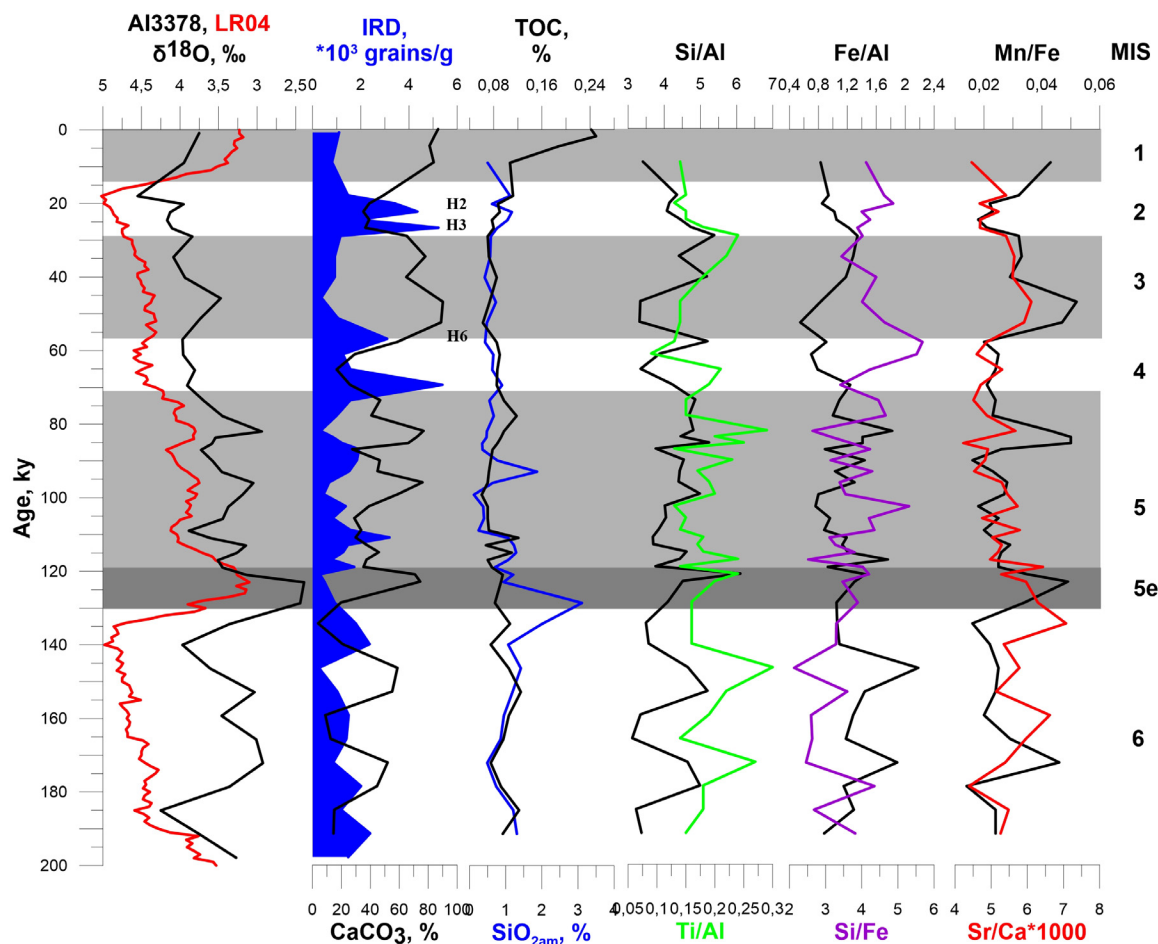


**Figure 3.** Stable oxygen isotope ratios (‰) in planktonic foraminiferal tests; LR 04 - standard curve [38], ice-rafted debris (IRD,  $10^3$  grains/g);  $\text{CaCO}_3$  (%); TOC ( $C_{\text{org}}$ )%;  $\text{SiO}_{2\text{am}}$  (%); and elemental ratios Si/Al, Ti/Al, Fe/Al, Si/Fe, Mn/Fe, and (Sr/Ca)1000 in AI-3378 sediment core (the Snorri Drift). Colored fill indicates the interglacial stages. H2 H3, and H6 are the Heinrich events.

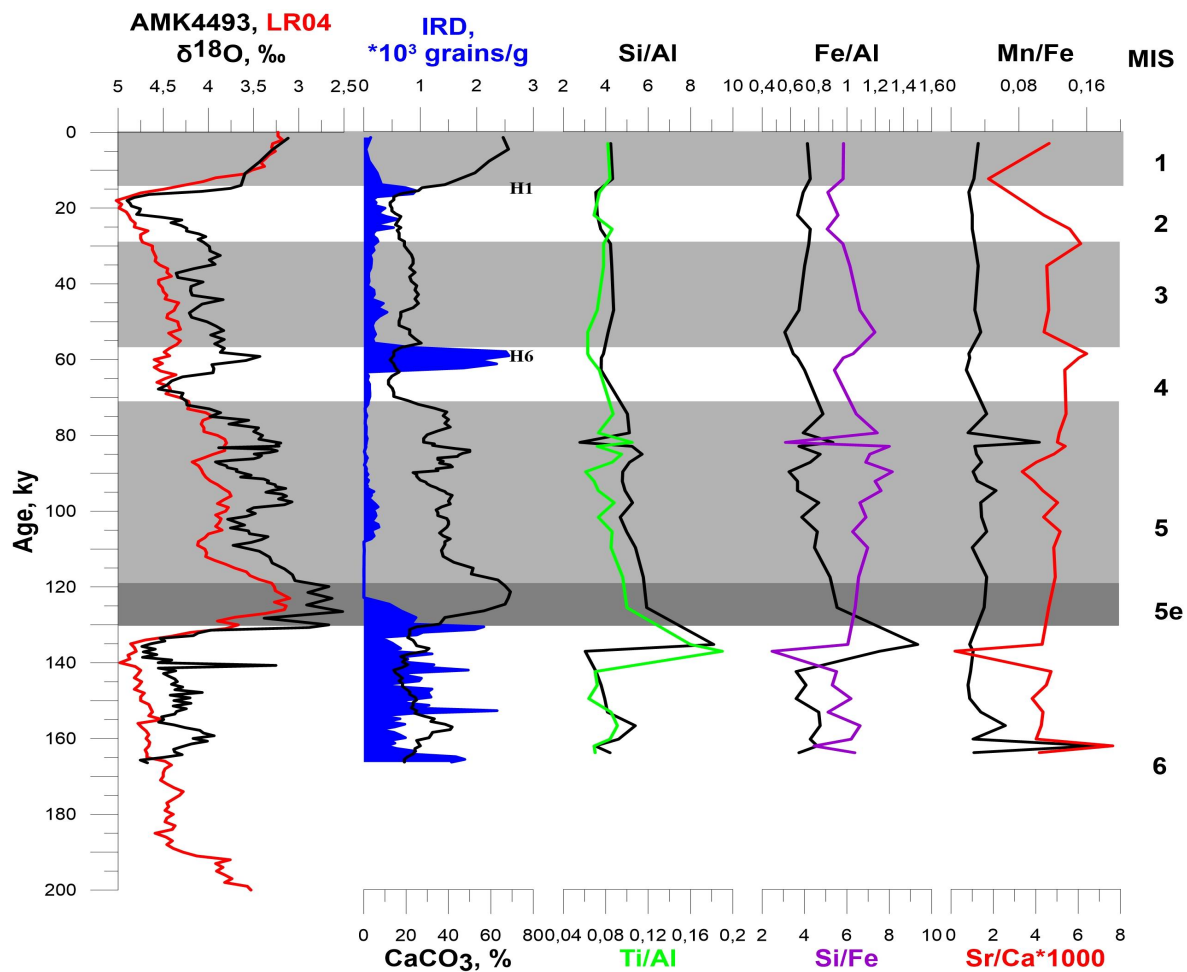


**Figure 4.** Stable oxygen isotope ratios (‰) in planktonic foraminiferal tests; LR 04\_- standard curve [38]; ice-rafted debris (IRD, (grains/g);  $\text{CaCO}_3$  (%); and elemental ratios Si/Al, Ti/Al, Fe/Al, Si/Fe, Mn/Fe, and  $(\text{Sr/Ca})1000$  in AMK-4493 sediment core (the Gloria Drift). Colored fill indicates the interglacial stages. H1 and H6 are the Heinrich events.

### 3.2. Elemental Analysis

The content of chemical elements in bulk bottom sediments (Al, Si, Ca, Mg, K, Fe, Mn, Ti, P, Cr, Sr, Zr, V, Rb, Ba) was carried out by X-ray fluorescence method (XRF). The Spectroskan MAK-S-GVM (SPEKTRON, St. Petersburg, Russia) equipped with a vacuum spectrometry chamber (four crystals: LiF200, C002, PET, and KAP, in the mode of 40 kV, from 0.50 to 2.0 mA) was used. Before measurements, sediment samples were dried (at 105 °C during 8 hours) and powdered in the Fritsch Planetary Mill Pulverisette 5/4 classic (Germany). Using a hydraulic press, specimens were tableted in special cups with the addition of powder of boric acid. Each sample was measured twice. The accuracy of measurements was controlled using the certified reference material (CRM) SDO-1 (terrigenous clay), SDO-3 (carbonate sediment), and NIST-2703 (marine sediment). Accuracy varied within the limits of  $\pm 12\%$ ; the reproducibility of major elements' analysis changed from 0.1 to 2.3%, while that for trace elements from 5.6 to 10.5%.

## 4. Results

### 4.1. Biogenic Components ( $\text{CaCO}_3$ , TOC, $\text{SiO}_{2am}$ ) and Ice-Rafted Debris

The  $\text{CaCO}_3$  content in marine sediments is mainly controlled by the surface water biological productivity, so it is usually used as a proxy of paleo productivity of seawater during sedimentation.

The  $\text{CaCO}_3$  content varies within the limits of 4–90% and 12–69% for AI-3378 and AMK-4493 cores respectively; such values are typical of the North Atlantic pelagic sediments [35,36]. From Figures 2 and 3, it follows that the down-core variations in  $\text{CaCO}_3$  and the  $\delta^{18}\text{O}$  values are very similar: Their elevated values are recorded during the relatively warm MIS 1, 3, and 5e, while the decreased values, on the contrary, are recorded during the colder MIS 2, 4, and 6. The lowest  $\text{CaCO}_3$  values (< 5%) were detected for AI-3378 core in the cooling period of MIS 6 (Figures 3 and 4). In both cores, the warmest period MIS 5e is distinguished by the peaks in  $\text{CaCO}_3$  (around 90%) and  $\delta^{18}\text{O}$  (3‰) values. These proxies have been studied in detail [15,34].

Maximum IRD values (up to 5000 grains/g sediment) were recorded in the Snorri Drift during MIS 2 and 4 cooling periods (Figures 3 and 4). This may indicate an additional input of terrigenous material during stadials, reflecting an increase in the volume of icebergs. The lowered values of IRD contents (from 0.3 to 1–3 thou. grains/g sediment) characterize sediments of MIS 1, 3, 5e and some interstadials of MIS 5 corresponding to relative warming.

The TOC content in the AI-3378 core varies around 0.1% and increases up to 0.24% only in the uppermost layer (0–20 cm), which we ascribed to MIS 1 of the Holocene (Figure 3). Amorphous silica is a well-known building material for diatoms valves and silicoflagellates, as well as zooplankton (radiolarians and sponges), i.e. biogenic  $\text{SiO}_2$  ( $\text{SiO}_{2\text{am}}$ ) can serve as an indicator of paleo-productivity of seawater. According to our data (Figure 3), concentrations of biogenic silica distinctly increase, amounting up to 25–50% of bulk Si during transition periods (MIS 6/5, 2/1). The maximum  $\text{SiO}_{2\text{am}}$  content (up to 3%) was found at a depth of 360 cm, supposedly ascribed to the beginning of MIS 5e. This maximum can be explained by migration of the Polar Front (PF) to the studied area during deglaciation, when, as is well known, productivity increased along the boundary of the hydrological fronts. This can also explain the second peak of biogenic  $\text{SiO}_{2\text{am}}$  (~2%) at a depth of 230 cm (MIS 5a?). In both cases, the increase in  $\text{SiO}_{2\text{am}}$  coincides with a decrease in calcium carbonate, which may indicate an entry of cold freshened waters into the studied area. For comparison, in the AMK-4453 core, also recovered on the Snorri Drift [15], the downcore decrease in IRD grains and elevated values of the sorted fine silt indicator (SS 18–23  $\mu\text{m}$ ), which correspond to the period of intensified contour currents during MIS 1, 3, and 5e, have been revealed.

#### 4.2. Chemical Elements

Contents of chemical elements (average value for each sample) in sediment cores at the Snorri (AI-3378, n = 46) and Gloria (AMK-4493, n = 37) Drifts are listed in Tables 1 and 2 respectively.

**Table 1.** Counts of IRD,  $\delta^{18}\text{O}$ , contents of  $\text{CaCO}_3$ , major and trace elements in sediment core AI-3378, the Snorri Drift [36].

Sed. Depth	IRD	$\delta^{18}\text{O}$	$\text{CaCO}_3$	Mg	Al	Si	K	Ca	Ti	Mn	Fe	P	V	Cr	Zn	Rb	Sr	Zr
(cm)	(grains/g)	(Permil VPDB)	(%)	(%)	(%)	(%)	(%)	(%)	(%)	(%)	(%)	(%)	(ppm)	(ppm)	(ppm)	(ppm)	(ppm)	(ppm)
0–1	1097	3.75	-	-	-	-	-	-	-	-	-	-	-	-	-	-	-	-
10–11	805	3.95	83.8	0.95	1.96	6.68	0.24	40.31	0.28	0.069	1.62	0.048	76	45	32	16	1799	90
20–21	1465	4.55	49.0	1.42	3.63	15.79	0.73	16.51	0.53	0.108	3.42	0.062	107	52	76	40	894	126
30–31	3417	3.95	39.2	2.09	4.83	20.00	0.87	11.72	0.63	0.092	4.11	0.062	119	55	93	56	549	140
40–41	4347	4.13	35.1	1.99	4.69	19.10	0.82	12.13	0.70	0.108	4.77	0.070	125	43	88	48	631	131
50–51	1894	4.17	39.2	1.49	4.00	17.72	0.83	14.88	0.61	0.077	4.19	0.053	112	58	89	58	699	169
60–61	5223	4.10	36.5	1.33	3.82	18.10	0.79	15.04	0.67	0.100	4.67	0.040	126	57	83	45	706	223
70–71	1153	3.84	65.2	1.51	2.33	12.54	0.51	22.39	0.56	0.100	3.12	0.040	109	28	48	22	1211	106
80–81	919	4.09	78.0	1.14	1.83	8.06	0.34	27.32	0.41	0.077	2.34	0.044	84	26	28	16	1542	106
90–91	918	3.94	64.8	1.16	2.26	11.70	0.55	22.39	0.40	0.077	2.66	0.040	89	31	43	31	1252	84
102–103	361	3.47	90.1	1.04	1.78	5.94	0.24	29.34	0.25	0.077	1.48	0.044	73	44	28	11	1793	69
112–113	1049	3.74	88.9	1.01	1.83	6.07	0.27	29.30	0.25	0.062	1.31	0.044	68	33	25	13	1732	76
122–123	3095	3.97	58.7	1.36	2.47	12.83	0.60	22.17	0.33	0.046	2.26	0.053	85	40	61	38	1082	140
130–131	1253	3.96	29.2	1.65	5.15	19.98	1.04	10.89	0.46	0.092	3.62	0.075	87	39	87	79	501	133
140–141	1566	3.81	16.7	2.03	6.48	21.68	1.03	7.14	0.73	0.123	5.12	0.070	128	55	98	79	379	126
150–151	5386	3.91	26.0	1.69	4.85	20.43	0.82	11.05	0.92	0.123	5.99	0.044	155	74	87	63	516	145
160–161	1565	3.69	46.8	1.45	3.24	15.73	0.65	17.89	0.50	0.085	3.53	0.035	104	51	75	40	807	141
170–171	1000	3.45	40.7	1.37	3.75	17.58	0.76	15.62	0.55	0.085	3.77	0.040	109	64	72	55	763	87
180–181	323	2.94	76.8	1.25	1.94	9.32	0.37	25.84	0.56	0.154	3.53	0.031	106	45	63	19	1465	80
190–191	829	3.54	72.1	1.18	2.06	9.17	0.36	25.98	0.42	0.139	2.90	0.035	98	19	28	20	1292	89
200–201	1221	3.59	66.1	1.22	2.06	10.79	0.39	25.15	0.52	0.146	2.91	0.040	92	43	27	21	1064	118
210–211	1924	3.73	27.4	1.70	5.03	18.93	0.85	11.19	0.64	0.116	4.47	0.057	111	47	94	57	549	167
220–221	1839	3.58	46.5	1.53	3.40	15.43	0.67	17.44	0.79	0.077	4.91	0.026	122	58	134	45	842	174
230–231	1515	3.46	45.0	1.63	3.86	17.09	0.79	15.53	0.67	0.092	3.98	0.048	125	58	83	39	704	103
240–241	685	3.05	76.1	0.97	1.92	8.44	0.36	26.80	0.37	0.069	2.49	0.035	125	14	19	22	1419	95
250–251	459	3.19	58.9	1.16	2.60	12.96	0.61	21.38	0.53	0.100	3.65	0.035	117	42	48	39	1165	70
260–261	1375	3.37	39.0	1.73	4.55	18.27	0.86	13.10	0.58	0.062	3.44	0.040	113	42	74	58	751	100
270–271	828	3.45	28.9	1.71	4.87	19.71	0.83	11.35	0.73	0.116	4.69	0.048	134	64	78	60	539	93
280–281	1573	3.89	33.6	1.99	5.52	21.21	0.96	9.83	0.79	0.100	4.87	0.044	140	64	75	56	569	144
290–291	3190	3.60	29.8	1.90	5.32	19.60	0.89	10.48	0.98	0.146	6.31	0.040	180	82	86	55	527	131
300–301	1466	3.15	37.4	1.87	5.12	18.92	0.85	11.24	0.89	0.169	5.78	0.044	154	70	88	50	595	146
310–311	1264	3.26	45.8	1.35	3.47	16.02	0.69	16.98	0.64	0.108	4.21	0.040	125	64	59	46	882	160
320–321	779	3.51	37.4	1.58	4.28	18.96	0.77	13.49	1.04	0.192	7.53	0.026	150	91	141	54	671	124
330–331	1728	3.45	35.3	1.93	5.51	20.71	0.92	9.92	0.80	0.131	5.14	0.066	143	70	93	59	638	185



**Table 2.** Counts of IRD,  $\delta^{18}\text{O}$ , contents of  $\text{CaCO}_3$ , major and trace elements in sediment core AMK-4493, the Gloria Drift.

Sed. Depth	IRD *	$\delta^{18}\text{O}$ *	$\text{CaCO}_3$	Al	Si	K	Ca	Ti	Mn	Fe	P	Cr	Rb	Sr	Zr
(cm)	(grains/g)	(permil VPDB)	(%)	(%)	(%)	(%)	(%)	(%)	(%)	(%)	(%)	(ppm)	(ppm)	(ppm)	(ppm)
2	35	3.30	68.3	5.15	21.80	1.82	9.07	0.42	0.120	3.73	0.062	42	100	420	123
8	310	3.64	38.3	4.51	19.43	1.63	23.79	0.38	0.092	3.34	0.057	50	79	424	127
14	868	4.66	17.5	6.38	22.50	2.16	11.52	0.47	0.092	4.41	0.075	50	114	316	120
30	394	4.52	17.5	6.12	22.02	2.09	6.30	0.42	0.100	3.95	0.077	43	103	275	127
40	210	4.24	15.8	6.19	23.27	2.11	6.38	0.53	0.116	4.59	0.070	47	118	357	128
50	248	4.05	19.2	5.36	22.64	1.91	6.50	0.42	0.108	3.90	0.062	49	104	398	122
60	152	3.99	19.2	5.12	21.92	1.84	8.63	0.40	0.116	3.57	0.062	50	99	390	125
80	121	4.16	21.7	5.44	23.74	1.93	7.90	0.39	0.100	3.59	0.062	45	105	364	145
90	408	4.21	17.5	5.43	22.34	1.98	8.83	0.34	0.108	3.05	0.062	33	94	388	124
100	206	3.97	21.7	6.55	25.47	2.09	4.69	0.41	0.085	4.05	0.077	42	127	300	166
102	2567	3.43	14.2	6.43	24.34	2.11	5.38	0.42	0.092	4.17	0.077	43	129	325	149
108	1992	3.59	12.5	6.24	23.59	2.24	6.26	0.46	0.077	4.36	0.097	45	125	336	125
130	52	3.98	37.5	3.35	17.83	2.05	16.11	0.29	0.116	2.77	0.053	39	86	875	87
140	36	3.40	30	4.00	20.44	1.89	13.11	0.29	0.054	2.75	0.057	38	91	670	122
145	36	3.40	30	1.91	5.31	0.38	28.17	0.20	0.177	1.71	0.106	32	14	1413	80
150	42	3.20	28.3	3.72	19.55	1.77	14.72	0.28	0.069	2.45	0.053	34	82	793	89
160	24	3.41	45	2.84	16.22	1.44	18.49	0.27	0.069	2.29	0.048	32	65	899	92
170	23	3.88	35.8	3.70	18.95	1.71	14.50	0.32	0.100	2.75	0.053	38	82	585	110
180	23	3.88	35.8	4.46	21.42	1.92	11.15	0.27	0.069	2.63	0.057	32	95	375	133
190	72	3.53	25	4.48	21.41	1.60	11.28	0.31	0.092	2.92	0.057	50	101	441	130
200	68	3.35	29.2	4.23	20.77	1.90	12.39	0.31	0.146	2.73	0.057	35	96	536	107
210	176	3.36	38.3	3.62	19.04	1.86	14.85	0.32	0.100	2.88	0.057	43	87	747	100
220	202	3.16	40.8	3.82	17.88	1.70	14.29	0.28	0.092	2.59	0.053	34	72	624	92
230	182	3.79	39.2	3.65	18.18	1.69	14.93	0.31	0.123	2.90	0.057	38	86	769	106
240	155	3.55	35.8	3.53	19.06	3.45	15.05	0.30	0.069	2.73	0.057	37	81	730	111
250	8	3.44	36.7	2.09	12.06	1.12	23.37	0.20	0.077	1.84	0.044	34	48	1151	66
260	2	3.04	63.3	2.10	12.47	1.16	23.00	0.21	0.077	1.95	0.048	30	49	1063	100
280	572	4.74	25	2.30	20.91	1.88	11.28	0.37	0.077	3.46	0.057	48	95	485	122
285	406	4.72	29.2	6.89	20.88	1.06	5.21	1.31	0.223	8.47	0.132	149	53	576	160
300	789	4.50	15	6.28	22.28	2.12	7.04	0.44	0.092	4.04	0.062	39	100	332	102
310	470	4.29	18.3	5.93	22.41	2.24	7.29	0.43	0.085	4.22	0.062	45	126	328	127
320	777	4.38	25	5.44	21.49	2.33	8.85	0.35	0.077	3.47	0.062	39	108	339	95
330	836	4.37	24.2	5.18	21.14	2.15	9.56	0.44	0.146	4.14	0.062	44	113	415	125
340	544	4.26	41.7	3.40	18.34	1.73	15.82	0.31	0.177	2.77	0.057	36	78	674	144
350	453	4.01	25	4.74	21.82	2.02	10.79	0.40	0.092	3.52	0.062	42	98	434	112
355	393	4.29	26.7	6.08	21.26	0.93	6.54	0.42	0.816	4.78	0.092	51	52	499	94
360	792	4.29	23.3	5.26	22.10	2.11	9.20	0.37	0.092	3.47	0.062	39	99	384	105

Notation: \* data from [20].

At the Snorri and Gloria Drifts, the lower and minimal contents of elements associated with aluminosilicates' supply, such as Al, Si, K, Ti, Cr, and Zr, were detected during the interglacial sediments (MIS 1, 3, 5), while, vice versa, their higher and maximal contents were detected in the glacial periods (MIS 2, 4, 6). Coarse-grained fraction, which includes IRD, is undoubtedly the result of the iceberg transport of sedimentary material. All peaks of lithogenic element contents correspond to peaks of IRD.

Elevated contents of Ca, Sr, Mn, and P are characteristic for the interglacial periods (MIS 1, 3, and 5). A few peaks of high Ca and Sr contents are detected in the Holocene (0–10 cm), MIS 3, and MIS 5e, i.e., during the hydrobiological optimum (warming and increase in water productivity).

In the glacial sediments (MIS 2, 4, 6), Ca and Sr are deficient compared to the interglacial sediments formed in warmer periods. The downcore Ca content variations reach 20-fold, this corresponds to the strong variability of CaCO<sub>3</sub> content throughout the sediment cores over all the MIS stages, as shown above. Throughout the Gloria and Snorri Drifts cores, there is a rhythmic alternation of the high and low contents of Al, Si, Ti, Cr, and Zr; trends of their variation are asynchronous to that of Ca, Sr, Mn, and P. Since sediments studied are enriched in carbonates (average CaCO<sub>3</sub> content amounts 45.5 and 29.1% in cores AI-3378 and AMK-4493 respectively), the element averages were recalculated on the carbonate free basis (Element<sub>cfb</sub>). These values, as well as an average upper crust values [42], are listed in Table 3.

**Table 3.** Chemical element averages for the sediment cores of the Snorri and Gloria drifts and the upper crust [42].

Measure Units	Element	Snorri Drift	Gloria Drift	Upper Crust [38]
wt. %	Si	16.20	19.89	28.8
	Si <sub>cfb</sub>	30.39	28.00	
	Al	3.97	4.56	7.96
	Al <sub>cfb</sub>	7.45	6.42	
	Fe	4.48	3.38	4.32
	Fe <sub>cfb</sub>	8.40	4.76	
	Ca	16.44	11.95	3.85
	K	0.70	1.82	2.14
	K <sub>cfb</sub>	1.31	2.56	
	Ti	0.68	0.37	0.40
	Ti <sub>cfb</sub>	1.28	0.52	
	Mn	0.12	0.12	0.07
	Mn <sub>cfb</sub>	0.22	0.17	
	ppm	Zr	nd	114
Zr <sub>cfb</sub>		nd	160	
Sr		860	577	333
Sr <sub>cfb</sub>		1613	813	
Cr		58	43	126
Cr <sub>cfb</sub>		109	61	
V		123	nd	98
V <sub>cfb</sub>		231	nd	
Ba		373	nd	378
Ba <sub>cfb</sub>		709	nd	

Notation: cfb means elements contents recalculated on carbonate free basis; nd means no data.

The average contents of Si, Al, and Mn (on carbonate free basis) are similar in sediments of the Gloria and Snorri Drifts, while the latter are relatively enriched in Ti, Fe, Cr, Ca, and Sr. When element averages in both cores are compared to the upper crust contents, one can see that there is no significant difference between Al and Si content, while the drift cores are distinctly enriched (1.5–2.5-fold) in Ti, Fe, Mn, Ba, V, Ca, and Sr. We may suggest that an additional contribution of Ti, Fe, and V into the area studied resulted from sedimentation of the aeolian dust which was enhanced during glacial periods [43]; Fe and V were probably derived from the fallout of the Icelandic volcanic dust onto the

sea ice which then was carried to the Labrador sea by the prevailing surface currents. The X-ray data on Ca contents, which are as much as three to four times higher compared to the upper crust, SEM and microscopy analysis of smear-slides, showed the abundance of foraminiferal and coccolithophore tests in our specimens and allowed us to suggest that elevated contents of Ca, Sr, and Mn were caused by their predominant accumulation in the biogenic carbonates whose abundance increased during warming periods.

The most significant relationships between chemical elements (based on data of regression analysis, Statistica 7 software) are listed in Table 4.

**Table 4.** Pair correlation coefficients ( $p < 0.05$ ) between some elements in the Snorri (st. AI-3378) and Gloria (st. AMK-4493) drift sediment cores.

Elements	Snorri Drift ( $n = 45$ )	Gloria Drift ( $n = 37$ )
Si–Al	0.88	0.65
Al–Fe	0.66	0.62
Al–Ti	0.68	0.38
Al–Ca	−0.89	−0.73
Ca–Si	−0.94	−0.80
Ca–Sr	0.79	0.71
$\delta^{18}\text{O}$ –IRD	0.48	0.20
$\text{CaCO}_3$ –IRD	−0.46	−0.49
Al–IRD	0.39	0.49
Si–IRD	0.45	0.40
Ti–IRD	0.17	0.22
Zr–IRD	0.63	0.30
$\text{CaCO}_3$ – $\delta^{18}\text{O}$	−0.08	−0.54
$\text{CaCO}_3$ –Al	−0.95	−0.60
$\text{CaCO}_3$ –Si	−0.98	−0.52
$\text{CaCO}_3$ –Ti	−0.35	−0.26
$\text{CaCO}_3$ –Zr	−0.55	−0.30
Al– $\delta^{18}\text{O}$	0.08	0.52
Si– $\delta^{18}\text{O}$	0.09	0.45
Ti– $\delta^{18}\text{O}$	−0.10	0.52
Zr– $\delta^{18}\text{O}$	0.38	0.37

A positive significant correlation in the Snorri and Gloria cores, respectively, was found for Si–Al ( $R^2 = 0.88$  and  $0.65$ ), Al–Ti ( $R^2 = 0.68$  and  $0.44$ ), Al–Fe ( $R^2 = 0.66$  and  $0.62$ ), and Ca–Sr ( $R^2 = 0.94$  and  $0.71$ ). The revealed statistically significant negative correlations between Al–Ca ( $R = -0.89$  and  $-0.83$ ), Al– $\text{CaCO}_3$  ( $-0.95$  and  $-0.60$ ), Si–Ca ( $R = -0.94$  and  $-0.80$ ), and Si– $\text{CaCO}_3$  ( $-0.98$  and  $-0.52$ ) in sediment cores of the Snorri and Gloria Drifts respectively, likely suggest a predominant Ca incorporation in biogenic carbonate rather than in terrigenous material. The examination of sediment specimens on SEM and smear slides under a POLAM L-213M polarizing microscope has revealed an insignificant amount of detrital calcite. In the southwest part of the area studied, a rather noticeable portion of Ca (up to 8%) occurred in the form of detrital carbonate (dolomite, limestone) related to discharge from northwestern Canada [44]. For Fe–Mn, a significant correlation ( $R^2 = 0.66$ ) was detected only in the Snorri Drift core.

## 5. Discussion

In the North Atlantic, Quaternary records are characterized by the frequent input of IRD and associated slowdown of deep-circulation [14,45]. The warm periods are characterized by the increased intensity of near-bottom currents, while in glacial ones, their speeds decreased. Sediment layers enriched in the IRD are distinguished by dominance of the coarse-grained fractions ( $> 150$ – $250 \mu\text{m}$ ) which have been supplied by melting icebergs over a vast area in the North Atlantic [22]. These layers are commonly depleted in Al content, and therefore, values of Si/Al, Ti/Al, and Fe/Al ratios may be

used as potential proxies of terrigenous contribution [21]. The percentage of sand grains in the North Atlantic sediments, used to identify the ice-rafting events, displayed a distinct coherent variability with quartz/plagioclase ratios, namely an increase during the glacial period, while the geochemical indicator (Ti/K ratio) showed the opposite trend [14]. These authors have found that the maximum warming period followed IRD deposition after increasing ventilation, as indicated by the  $\delta^{13}\text{C}$  of *N. pachyderma*. Ameliorated conditions for benthic foraminiferal environment were reflected by a relatively high Si/Fe, while a distinct drop in Al, Si, and K content and a drop in Si/Fe ratio suggests that less clay-mineral-loaded meltwater reached the area on the West Greenland shelf [46]. Based on surface temperature from planktonic foraminiferal count, Mg/Ca and oxygen isotopes of *Neogloboquadrina pachyderma*, and from  $\text{CaCO}_3$  content, the rapid shifts from cold stadial to warm interstadial caused by variable freshwater input by melting ice during MIS 3, have been revealed [14]. According to these authors, this variability was caused by changes in Atlantic Meridional Overturning Circulations (AMOC). The Ti/K ratio, which reflects the continental crust versus Mid-Atlantic Ridge basalt-derived material, serves as an indicator of continentally derived IRD; a decrease in Ti/K ratio suggests major changes in the provenance and transport way of sedimentary material. The Ti/Al ratios' distribution in the surface North Atlantic sediments supports its use as a proxy for aeolian versus fluvial input of terrigenous material [47]. The distributions of the Fe/K and Al/Si ratios in Atlantic surface sediments are highly similar to those of major soil types in Africa and South America. This result indicates the deposition on Atlantic continental margins of terrigenous material originating from the adjacent continent. In addition, the Fe/K and Al/Si ratios of Atlantic sediments reflect the relative input of terrigenous material from climatic zones characterized by different degrees of chemical continental weathering. High values indicate the dominant input of highly weathered material derived from tropical humid regions, while low Fe/K and Al/Si values reflect the input of only slightly chemically weathered material formed under drier conditions [47].

Maximal IRD deposition (2.566 grains/g of sediment) occurred at a horizon of 100–101 cm, close to termination of the cold MIS 4 (Figure 4) at the Gloria Drift. At this horizon, the 60% maximum of coarse silt fraction (250–125  $\mu\text{m}$ ) was detected [20]. However, this peak did not coincide with the highest values of Si/Al, Ti/Al, and Fe/Al ratios. The single peak value of Si/Al (8.6), Ti/Al (0.18), and Fe/Al (1.50) ratios, which were 4–5 times more compared to their core averages, were recorded at the Gloria Drift during the coldest glacial period MIS 6 at a horizon of 280–290 cm. There, according to [15], the total amount of coarse-grained fraction (250–125  $\mu\text{m}$ ) amounted to 36%, i.e., significantly less than in horizon 100–110 cm (60%). From Figure 4, it is distinctly seen that at the Gloria Drift core, the downcore distribution patterns of Si/Al, Ti/Al, and Fe/Al ratios were more or less similar to that of IRD only during MIS 6. The large amplitude of these ratios' variations and correlation with IRD only in the coldest period confirm a common use of Si/Al, Ti/Al, and Fe/Al ratios, which refers to the contribution of coarse-grained material during the cold glacial periods. However, with the absence of a noticeable downcore variation in these ratios and IRD, let us suppose the existence of a powerful source of terrigenous fine-grained rather than only coarse-grained material supplied into sediments at the Gloria Drift area. In the works [15,33], the two large-scale deposition systems of material supplied by turbidite inflow from the Labrador Sea to the Gloria Drift, namely sand-dominated and mud-dominated, have been discovered. These systems operate under the influence of the submarine drainage system of the Northwest Atlantic Mid-Ocean Channel (NAMOC), and the grain size separation resulted from the sorting of glacial sediments.

In the AI-3378 site from the Snorri Drift (Figure 3), unlike the Gloria Drift core, multiple alternating of the elevated and lowered values of Si/Al, Ti/Al, and Fe/Al ratios was revealed. There, one can see a general similarity in the downcore distribution of the IRD terrigenous grains, Si/Al, Ti/Al, and Fe/Al ratios which was recorded throughout the core with rather small variations around the averages. Some peaks of these ratios were detected close to boundaries between MIS 2/3, 3/4, 5/5e, as well as during interglacials. On the one hand, these may indicate their common source related with the silt and fine-sandy fractions of terrigenous ice rafting material, whose abundance has been systematically

increased in cold periods, followed by the input of sedimentary matter by melting icebergs. On the other hand, we suppose in the Snorri Drift core such a rhythmic alteration of layers with relatively high and low Si/Al, Ti/Al, and Fe/Al ratios. These seem to be in agreement with a frequent systematic input of IRD grains in Northwest Atlantic sediments associated with the slowdown of deep circulations [45] and may be attributed to the influence of the coarse-grained ice-rafted debris during the colder periods. Besides, an impact of fine-grained terrigenous material (clays) brought with near-bottom currents, mainly the Iceland–Scotland Overflow Water (ISOW), should not be excluded. These near-bottom currents have been enhancing during interglacials, while their intensity is known to be oscillated regularly over the past time.

It should be noticed that there is no significant difference (around 10–15%) between average values of Si/Al for interstadial (MIS 1, 3, and 5) and stadial (MIS 2, 4, and 6) periods: 4.34 vs 4.13 in the Snorri Drift and 4.79 vs 4.24 in the Gloria Drift, respectively. The same tendency could be noticed on the Ti/Al ratio in cores and the Fe/Al ratio in the Gloria Drift. In the case of the Snorri Drift, during warmer MIS 1, 3, and 5, the average Fe/Al ratio (1.56) is significantly (about 25%) higher than that in the cooler MIS 2, 4, and 6. This may be attributed to an additional source of Fe caused by an enrichment in Fe of the Snorri Drift core (average Fe/Al is 1.18) relative to the upper crust (0.44, by [42]). Such an enrichment during warmer interstadials may be caused by bioturbation, whose traces we observed while describing the core. As is known, the effects of macrozoobenthos activity include biodeposition, particle reworking, solute exchange during bio-irrigation, and burrowing. Benthic–sediment interaction could be realized in different ways, for example, an increase of migration of the Fe bioavailable forms from pore water into sediment. From our experience, we have learnt that the major role in biogeochemical transformation of metals, particularly Fe as an essential element, belongs to benthic organisms enriched in organic carbon, such as polychaetes (a deposit feeders), whose fossilized tracks were found during visual observation of the cores. Besides, shells of carbonate-forming organisms (foraminiferas, coccolithophores, bivalves) have displayed a high accumulation of metals due to films of authigenic Fe–Mn oxyhydroxides being formed on their surface [48–50]. The latter phenomenon was observed in both shallow and deep-sea bottom environments [51].

In both cores, elevated values of Si/Al, Ti/Al, and Fe/Al ratios were generally coherent to lowered CaCO<sub>3</sub> content which is used as a biogenic proxy whose high content suggests the growth of surface water biological productivity (the foraminiferal assemblages mostly) during warmer periods. In case of the absence or insignificant contents of the detrital carbonates, changes in CaCO<sub>3</sub> are mostly provided by changes in productivity which in turn is driven by the temperature of surface water, as was shown by [52]. So, despite the lack of a significant coefficient of correlation ( $R^2$  did not exceed 0.22), we suppose that in the case of our cores, CaCO<sub>3</sub> is of predominantly biogenic origin. So, in this aspect, these ratios could be applied as terrigenous proxies of sediment formation in contourite drifts during the stadials.

A relatively high Si/Fe ratios and depleted  $\delta^{18}\text{O}$  values suggest warmer conditions from 6650 to 3800 cal.yr BP corresponding in time to Holocene Thermal Maximim, therefore, Si/Fe ratio is regarded in the North Atlantic as a proxy for the supply of clay-mineral-loaded glacial meltwater, which carry fine-grained sediments away from the slope [46]. In the Snorri and Gloria Drifts' cores, the Si/Fe ratio is 3.81 and 5.86 respectively, that is lower than that of the upper crust average (6.67, by [42]); it additionally confirms these sediments' enrichment in Fe compared to the upper crust as was mentioned above. The alteration of higher and lower values of Si/Fe ratios are also clearly displayed in the case of the Snorri Drift (Figure 3). Variations in Si/Fe ratios exhibit a general slight tendency of insignificant upward growth, with multiple oscillations, from the coldest MIS 6, where the minimal Si/Fe ratios (2.2) were detected, to the warm Holocene where this ratio reached 4.0. However, no significant difference was found between average values of Si/Fe in the relatively warm (3.85) and cold (3.75) periods. The high values of the Si/Fe ratio (5.5 to 6) were registered in the beginning of the warm MIS 5, at the boundaries MIS 5/4, as well in relatively warm MIS 3. The amplitude of Si/Fe ratios' variation in the Snorri Drift (3.1 to 5.6) is less than that in the Gloria Drift (2.0 to 7.7). Throughout the Gloria Drift

core, only the two distinct minimal Si/Fe ratio' values were recorded, in the cold MIS 4 and 6 (2.8 and 2.2 respectively), as it was shown above for Si/Al, Ti/Al, and Fe/Al ratios. In the Gloria Drift core, it is interesting to notice that the strongly pronounced minimum Si/Fe ratio, observed at the horizon of 370–380 cm during cold MIS 6, corresponds to the maximum of Si/Al, Ti/Al, and Fe/Al ratios. Besides, we found no change in Si/Fe ratios corresponding to detected high values of  $\delta^{18}\text{O}$  and  $\text{CaCO}_3$  during the warm MIS 5 (Figure 4). In both cores, the Si/Fe ratios exhibit an asynchronous downcore distribution with that of Si/Al, Ti/Al, Fe/Al, and IRD. On the contrary, generally coherent variations were revealed for Si/Fe ratios,  $\delta^{18}\text{O}$ , and  $\text{CaCO}_3$ .

Thus, the Si/Fe ratio as a proxy of the clay-mineral-loaded glacial meltwater, in our opinion, is more applicable for the transition periods between cold and warm periods.

As is well known, the Mn cycles reflect the extent of sediment oxidation resulting from changes in ventilation of bottom water, reflecting bulk sedimentation rate and terrigenous versus biogenic supply. The high contents of Mn oxides are characteristic for strongly oxidizing conditions, while under suboxic conditions, Mn oxyhydroxides are dissolved. The Mn/Fe ratio is usually applied for the paleoreconstruction of oxygen dynamics in the bottom waters [29]. This is caused by the different redox kinetics of Mn and Fe under anoxic conditions, namely, Mn is reduced faster than Fe, while Fe is oxidized faster than Mn; therefore, a higher Mn/Fe ratio characterizes suboxic or oxic conditions. A trend of the relatively high Mn/Fe ratios in the warm MIS 1, 3, 5, 5e is clearly observed in the Snorri Drift core. Hence, we may suggest that during warmer periods, an efficiency of the Mn diagenetic transfer into Mn (IV) state was higher relative to Fe, resulting in elevated Mn/Fe ratios in sediments.

So, Mn/Fe ratios variations apparently reflect the redox conditions of the paleoenvironment. In the western Arctic Ocean sediment cores, enriched in the Mn brown units were attributed to the glacial intervals, while the clear mechanisms of such correlation is still speculative [26]. In the subpolar White Sea (Northwestern Russia), a change in the Mn/Fe ratio in mobile forms (exchangeable and oxyhydroxides) reflects the rapid oxidation of Mn (II) in the uppermost layers of the cores, as well as a slowdown of diagenetic reduction of the oxidized forms of Fe and Mn at a depth of ~130 cm [30,53].

According to our data, in cores from the Snorri and Gloria Drifts, higher values of Mn/Fe ratios generally corresponded to lower IRD deposition in warmer periods, while in cooler times, Mn/Fe ratios decreased (Figures 3 and 4). A comparison of average Mn/Fe ratios has shown a significant difference in warmer (0.033 and 0.074) versus colder (0.023 and 0.035) periods in the Snorri and Gloria Drifts cores respectively.

The distinct Mn/Fe peaks were recorded in the Holocene MIS 1; in interglacial sediments formed during MIS 3, 5, and 5e; as well as in glacial period MIS 6. It should be noticed that in the Snorri Drift, the downcore changes of the Mn/Fe ratio are similar to that of  $\text{CaCO}_3$ , and to a lesser extent, to  $\delta^{18}\text{O}$  (Figure 3). We suppose that it may be caused by the incorporation of Mn into carbonate material whose vertical fluxes increased in warmer periods due to the growth of biological productivity. In the case of the Gloria Drift, the downcore Mn/Fe variation is almost absent, with the exception of two large peaks in the stadials MIS 4 (horizon of 150 cm, about 77,320 yrs. ago) and MIS 6 (horizon of 350 cm, about 185,320 yrs. ago). We suppose that it was caused by an abrupt and short onset of very strong oxidation conditions resulting from enhanced water ventilation which may be linked to inflowing of the cold East Greenland Current.

Some marine isotope stages such as MIS 3 and 5 are usually sub-divided into sub-stages in accordance with peaks of glacial or interglacial basic parameters related to ice-rafting events versus biogenic supply. This sub-division is supported by our data, displaying several peaks in downcore record of chemical elements and some of their ratios.

The changes in Sr/Ca ratios in planktonic and benthic foraminifera from diverse hydrographic settings over 300 kyr, revealed an increase over the penultimate glaciation, declining to minimum values during MIS 5 and increasing from MIS 5 through MIS 2; these variations are explained by changes in mean Sr/Ca value in ocean water and only a small influence of salinity and pH, rather than temperature changes [54]. The Sr/Ca ratios in bulk sediments from gravity cores from the South

Atlantic Ocean displayed glacial/interglacial variations with minimum values during glacial maxima, a distinct increase in deglaciation periods, and the highest ratios in interstadials [31]. In accordance with Reference [55], the downcore Sr/Ca variations are influenced mainly by the recrystallisation of shelf aragonite into calcite, resulting in an increased Sr/Ca ratio during glacial maxima. Additionally, the variable Sr incorporation by carbonate-producing coccolithophores and foraminifers was suggested to vary on a species-to-species basis [56].

Our data displayed a rhythmic alteration of higher and lower Sr/Ca ratios, however, with no strongly pronounced peaks (Figures 3 and 4). At the Snorri Drift, the downcore change in Si/Al, Ti/Al, and Fe/Al ratios exhibits a general trend of asynchronous distribution with that of Sr/Ca ratios (Figure 3). In sediments of the Gloria Drift, this trend seems to be more pronounced (Figure 4). In both cases, the opposite trends in the down-core distribution of CaCO<sub>3</sub> and Sr/Ca ratios are clearly seen. Due to multiple and rhythmic alteration of the higher and lower (Sr/Ca) ratio values throughout the AMK-3378 core from Snorri Drift (Figure 3), there is no significant difference in warmer periods versus colder ones (5.37 and 5.24, respectively). However, at the Gloria Drift (AMK-4493 core), one can clearly see two sharp decreases in the Sr/Ca ratio: one is at the boundary MIS 2/1 and the second is in the MIS 6 at the horizon of 270–280 cm. The second minimum coincides with maximal values of terrigenous indicators, such as Si/Al, Ti/Al, and Fe/Al ratios, and high IRD values. Thus, we obtained ambiguous data on Sr/Ca records which cannot be ascribed to the paleoclimate indicators in the cores studied. From this, it follows that additional research should be further made by analyzing the individual foraminifer shells using standard methods.

## 6. Conclusions

Geochemical paleorecords of climate change during the Late Quaternary period have been considered. The results of quantitative XRF analysis combined with the IRD, CaCO<sub>3</sub>, oxygen isotopes, BioSiO<sub>2</sub>, and lithological characteristics of the sediment sequences of the Snorri and Gloria Drifts are presented. These sedimentary bodies have been formed as a result of the near-bottom contour currents, as well as ice melting and iceberg unloading, whose intensity and direction changed dramatically as was shown in many publications. The data obtained let us reveal the temporal variations in geochemical characteristics of the paleoenvironment in the North Atlantic during the Mid-Pleistocene to Holocene covering MIS 6 to MIS 1 (180–190 kyr BP). In both cores, the rhythmic peaks of IRD grains' content suggest a frequent systematic input of IRD grains in Northwest Atlantic sediments, these, in accordance to [45], are associated with slowdown of deep circulations. Major and trace element contents and some of their ratios exhibit their multiple and rhythmic variation over the glacial/interglacial periods. In both the Snorri and Gloria Drifts cores, the sediment records showed the downcore co-variation of ice-rafted debris (IRD) and terrigenous elements, such as Si, Al, Ti, Cr, and Zr contents. These downcore variations occurred asynchronously with biogenic components (CaCO<sub>3</sub> and BioSiO<sub>2</sub>), which are commonly used as a proxy of biological productivity (carbonate- and silicon-forming phyto- and zooplankton) of surface water, as well as  $\delta^{18}\text{O}$ . The warm MIS 3 and 5 are usually sub-divided into some sub-stages in accordance to peaks of glacial or interglacial basic parameters related to ice-rafting events versus biogenic supply. This sub-division is supported by our data, displaying several peaks in downcore record of chemical elements and some of their ratios.

Some elemental ratios may be used as proxies of climate change. An asynchronous alternation of high and low values of terrigenous and biogenous indicators seemed to result from changes in sedimentary material supplied to the studied area by ice and iceberg rafting, as well by bottom currents during warming and cooling periods. Elevated values of Si/Al, Ti/Al, and Fe/Al ratios were generally coherent to lowered CaCO<sub>3</sub>. The Si/Fe ratios exhibiting asynchronous downcore distribution with that of Si/Al, Ti/Al, Fe/Al, and IRD, used as a proxy of the clay-mineral-loaded glacial meltwater, in our opinion, is more applicable for the transition periods between cold and warm periods. The Mn/Fe ratio, reflecting the different kinetics of reduction-oxidation processes, exhibited the downcore co-variation with that of CaCO<sub>3</sub>, and to a lesser extent, to  $\delta^{18}\text{O}$ . These are possibly linked with the incorporation of

Mn into carbonate material whose vertical fluxes increased in warmer periods due to the growth of biological productivity. In the case of the Gloria Drift, the downcore Mn/Fe variation is almost absent, suggesting a general insignificant change in surface water productivity over the larger part of the core; however, the two large peaks recorded during MIS 4 and MIS 6, in our opinion, were caused by an abrupt and short onset of strong oxidation conditions that resulted from enhanced water ventilation, which may be linked to inflowing of the cold East Greenland Current.

**Supplementary Materials:** The following are available online at <http://www.mdpi.com/2076-3263/9/10/432/s1>, Table S1: The IRD counts,  $\delta^{18}\text{O}$ ,  $\delta^{13}\text{C}$ , contents (wt.%) of  $\text{CaCO}_3$  and TOC in sediment cores of the Snorri and Gloria drifts.

**Author Contributions:** L.L.D. performed XRF analysis and interpretation of the data set obtained; E.A.N. participated in the expedition sampling, made a division of the marine isotope stages based on biostratigraphic and oxygen isotope analysis, calculation of sedimentation rates; A.P.L. implemented the leadership of the RSF project over 2014–2018; N.V.K. has made a lithological description of the sediment cores on the ship board and mineralogical analysis.

**Funding:** This research was carried out in the framework a State Assignment of Ministry of Science and High Education, Russia (program no. 0149-2019-0007); field data were obtained in expedition supported by the Russian Science Foundation (<https://www.rscf.ru>), project no. 14-50-00095, “Interaction of Geospheres and Mineral Resources of the World Ocean”, led by Academician A.P. Lisitzin). Interpretation of some new data, as well as preparation of the manuscript were partially supported by the grant of the Russian Science Foundation, project no. 19-17-00234.

**Acknowledgments:** The authors are grateful to Vadim V. Sivkov and Leila D. Bashirova (both from the Atlantic Branch of Shirshov Institute of Oceanology, RAS) who provided us with  $\text{CaCO}_3$ ,  $\delta^{18}\text{O}$ , and IRD data for the AMK-4493 core, to N. Andersen for stable isotope analysis (Kiel University). The authors thank the crew of the R/V “Akademik Mstislav Keldysh” and R/V “Akademik Ioffe”, as well as all participants of the cruises for cooperation.

**Conflicts of Interest:** The authors declare no conflict of interests.

## References

1. Lappo, S.S. Warm advection to the north through equator in the Atlantic Ocean. In *Interaction of Ocean and Atmosphere*; Gidrometeoizdat: Moscow, Russia, 1984; pp. 125–129. (In Russian)
2. Broecker, W.S. The great ocean conveyor. *Oceanography* **1991**, *4*, 79–89. [[CrossRef](#)]
3. Gordon, A.H. Inter-ocean exchange of thermocline water. *J. Geophys. Res.* **1986**, *101*, 12217–12237. [[CrossRef](#)]
4. McManus, J.F.; Oppo, D.W.; Keigwin, L.D.; Cullen, J.L.; Bond, G.C. Thermohaline Circulation and Prolonged Interglacial Warmth in the North Atlantic. *Quat. Res.* **2002**, *58*, 17–21. [[CrossRef](#)]
5. Wright, A.K.; Flower, B.P. Surface and deep ocean circulation in the subpolar North Atlantic during the mid-Pleistocene revolution. *Paleoceanography* **2002**, *17*, 3–16. [[CrossRef](#)]
6. Lisitzin, A.P. *Sea-ice and Iceberg Sedimentation in the World Ocean: Present and Past*; Springer: Berlin, Germany, 2002; 563p.
7. Heezen, B.C.; Hollister, C.D.; Ruddiman, W.F. Shaping of the Continental Rise by Deep Geostrophic Contour Currents. *Science* **1966**, *152*, 502–508. [[CrossRef](#)] [[PubMed](#)]
8. Faugères, J.-C.; Stow, D.A.; Imbert, P.; Viana, A. Seismic features diagnostic of contourite drifts. *Mar. Geol.* **1999**, *162*, 1–38. [[CrossRef](#)]
9. Rebesco, M.; Stow, D. Seismic expression of contourites and related deposits: A preface. *Mar. Geophys. Res.* **2001**, *22*, 303–308. [[CrossRef](#)]
10. Rebesco, M.; Hernández Molina, J.; Van Rooi, D.; Wåhlin, A. Contourites and associated sediments controlled by deep-water circulation processes: State-of-the-art and future considerations. *Mar. Geol.* **2014**, *352*, 111–154. [[CrossRef](#)]
11. Thran, A.C.; Dutkiewicz, A.; Spence, P.; Müller, R.D. Controls on the global distribution of contourite drifts: Insights from an eddy-resolving ocean model. *Earth Planet. Sci. Lett.* **2018**, *489*, 228–240. [[CrossRef](#)]
12. Stoker, M.; Akhurst, M.; Howe, J.; Stow, D. Sediment drifts and contourites on the continental margin off northwest Britain. *Sediment. Geol.* **1998**, *115*, 33–51. [[CrossRef](#)]
13. Akhurst, M.C.; Stow, D.A.V.; Stoker, M.S. Late Quaternary glacialic contourite, debris flow and turbidite process interaction in the Faroe-Shetland Channel, NW European continental margin. *Geol. Soc. London Memoirs* **2002**, *22*, 73–84. [[CrossRef](#)]

14. Jonkers, L.; Moros, M.; Prince, M.A.; Dokken, T.; Anderssen Dahl, K.; Dijkstra, N.; Perner, K.; Brummer, G.-J.A. A reconstruction of sea surface warming in the North Atlantic during MIS 3 ice-rafting events. *Quater. Sci. Rev.* **2012**, *29*, 1791–1800. [[CrossRef](#)]
15. Sivkov, V.V.; Dorokhova, E.V.; Bashirova, L.D. Contour currents of the North Atlantic during the last glacial cycle. *Oceanology* **2015**, *55*, 899–905. [[CrossRef](#)]
16. Watkins, S.J.; Maher, B.A.; Bigg, G.R.; Maher, B. Ocean circulation at the Last Glacial Maximum: A combined modeling and magnetic proxy-based study. *Paleoceanography* **2007**, *22*. [[CrossRef](#)]
17. Bond, C.; Heinrich, H.; Broecker, W.; Labeyrie, L.; McManus, J.; Andrews, J.; Huon, S.; Jantschik, R.; Clasen, S.; Simet, S.; et al. Evidence of massive discharges of icebergs into the North Atlantic Ocean during the last glacial period. *Nature* **1992**, *360*, 245–249. [[CrossRef](#)]
18. Lubinski, D.J.; Polyak, L.; Forman, S.L. Freshwater and Atlantic water inflow to the deep northern Barents and Kara seas since ca 13 14C ka: Foraminifera and stable isotopes. *Quater. Sci. Rev.* **2001**, *20*, 1851–1879. [[CrossRef](#)]
19. Stow, D.A.V.; Faugères, J.-C.; Howe, J.A.; Pudsey, C.J.; Viana, A.R. Bottom currents, contourites and deep-sea sediment drifts: Current state-of-the-art. *Geol. Soc. Lond. Mem.* **2002**, *22*, 7–20. [[CrossRef](#)]
20. Bashirova, L.; Dorokhova, E.; Sivkov, V.; Novichkova, E. Paleotemperature, geochemical and grain size data in Quaternary sediments from the Gloria Drift (Northwest Atlantic). *Data Brief* **2018**, *19*, 758–761. [[CrossRef](#)]
21. Calvert, S.E.; Pedersen, T.F. Elemental proxies for palaeoclimatic and palaeoceanographic variability in marine sediments: Interpretation and application. In *Proxies in Late Cenozoic Paleooceanography*; Hillaire-Marcel, C., De Vernal, A., Eds.; Elsevier: Amsterdam, The Netherlands, 2007; Volume 1, pp. 568–643.
22. Henrich, H. Origin and consequences of cyclic ice rafting in the northeast Atlantic Ocean during the past 130,000 years. *Quat. Res.* **1988**, *29*, 142–152. [[CrossRef](#)]
23. Winkelmann, D.; Schafer, C.; Stein, R.; Mackensen, A. Terrigenous events and climate history of the Sophia Basin, Arctic Ocean. *Geochem. Geophys. Geosyst.* **2008**, *9*. [[CrossRef](#)]
24. Spofforth, D.J.A.; Pälke, H.; Green, D. Paleogene record of elemental concentrations in sediments from the Arctic Ocean obtained by XRF analyses. *Paleoceanography* **2008**, *3*, PA1S09. [[CrossRef](#)]
25. Polyak, L.; Bischof, J.; Ortiz, J.D.; Darby, D.A.; Channell, J.E.; Xuan, C.; Kaufman, D.S.; Løvlie, R.; Schneider, D.A.; Eberl, D.D.; et al. Late Quaternary stratigraphy and sedimentation patterns in the western Arctic Ocean. *Glob. Planet. Chang.* **2009**, *68*, 5–17. [[CrossRef](#)]
26. Jakobsson, M.; Løvlie, R.; Al-Hanbali, H.; Arnold, E.; Backman, J.; Mörrth, M. Manganese and color cycles in Arctic Ocean sediments constrain Pleistocene chronology. *Geology* **2000**, *28*, 23–26. [[CrossRef](#)]
27. Chester, R. *Marine Geochemistry*; Blackwell: London, UK, 2000; 506p.
28. Tribouillard, N.; Algeo, T.J.; Lyons, T.; Riboulleau, A. Trace metals as paleoredox and paleoproductivity proxies: An update. *Chem. Geol.* **2006**, *232*, 12–32. [[CrossRef](#)]
29. Naeher, S.; Gilli, A.; North, R.P.; Hamann, Y.; Schubert, C.J. Tracing bottom water oxygenation with sedimentary Mn/Fe ratios in Lake Zurich, Switzerland. *Chem. Geol.* **2013**, *352*, 125–133. [[CrossRef](#)]
30. Demina, L.L.; Bud'ko, D.F.; Alekseeva, T.N.; Novigatsky, A.N.; Filippov, A.S.; Kochenkova, A.I. Partitioning of trace elements in the process of early diagenesis of bottom sediments in the White Sea. *Geochem. Int.* **2017**, *55*, 144–149. [[CrossRef](#)]
31. Wien, K.; Kolling, M.; Schulz, H. Close correlation between Sr/Ca ratios in bulk sediments from the Southern Cape basin SPECMAP record. *Geo-Mar. Lett.* **2005**, *25*, 265–271. [[CrossRef](#)]
32. Sarafanov, H.; Falina, A.; Mercier, H.; Sokov, A.; Lherminier, P.; Gourcuff, C.; Gladyshev, S.; Gaillard, F.; Daniault, N. Mean full-depth summer circulation and transports at the northern periphery of the Atlantic Ocean in the 2000s. *J. Geophys. Res. Space Phys.* **2012**, *117*, 01014. [[CrossRef](#)]
33. Hesse, R.; Khodabakhsh, S. Significance of fine-grained sediment lofting from melt-water generated turbidity currents for the timing of glaciomarine sediment transport into the deep sea. *Sediment. Geol.* **2006**, *186*, 1–11. [[CrossRef](#)]
34. Novichkova, E.A.; Savvichev, A.S.; Bashirova, L.D.; Kozina, N.; Klyuvitkin, A.; Politova, N.V.; Novigatskii, N.; Lein, A. Lithological and biogeochemical investigations of the North Atlantic sediment system (data from the 49th cruise of the R/V Akademik Ioffe). *Oceanology* **2019**, *59*, 557–590. [[CrossRef](#)]
35. Lisitzin, A.P. *Processes of the Oceanic Sedimentation*; Nauka: Moscow, Russia, 1978; p. 392. (In Russian)
36. Barash, M.S. *Quaternary Paleooceanology of the Atlantic Ocean*; Nauka: Moscow, Russia, 1988; p. 254. (In Russian)

37. Elliot, M.; Labeyrie, L.; Bond, G.; Cortijo, E.; Turon, J.-L.; Tisnerat, N.; Duplessy, J.-C.; Turon, J.; Duplessy, J. Millennial-scale iceberg discharges in the Irminger Basin during the Last Glacial Period: Relationship with the Heinrich events and environmental settings. *Paleoceanography* **1998**, *13*, 433–446. [[CrossRef](#)]
38. Lisiecki, L.E.; Raymo, M.E. A Pliocene-Pleistocene stack of 57 globally distributed benthic  $\delta^{18}\text{O}$  records. *Paleoceanography* **2005**, *20*, PA1003. [[CrossRef](#)]
39. Sarnthein, M.; Stategger, K.; Dreger, D.; Erlenkeuser, H.; Grootes, P.; Haupt, B.J.; Jung, S.; Kiefer, T.; Kuhnt, W.; Pflaumann, U.; et al. Fundamental Modes and Abrupt Changes in North Atlantic Circulation and Climate over the last 60 ky—Concepts, Reconstruction and Numerical Modeling. In *The Northern North Atlantic*; Springer Science and Business Media LLC: Berlin, Germany, 2001; pp. 365–410.
40. Demina, L.L.; Novichkova, Y.A.; Kozina, N.V. Chemostratigraphy of the Snorrry Drift in the North Atlantic. *Oceanology* **2019**, *59*, 425–431. [[CrossRef](#)]
41. Gorbarenko, S.A.; Derkachev, A.N.; Astakhov, A.S. Lithostratigraphy and tephrochronology of upper quaternary sediments of the Sea of Okhotsk. *Russian J. Pac. Geol.* **2000**, *19*, 38–58.
42. Wedepohl, H. The composition of the continental crust. *Geochim. Cosmochim. Acta* **1995**, *59*, 1217–1239. [[CrossRef](#)]
43. Duce, R.A.; Tindale, N.W. Atmospheric transport of iron and its deposition in the ocean. *Limnol. Oceanogr.* **1991**, *36*, 1715–1726. [[CrossRef](#)]
44. Broecker, W.S.; Bond, G.; Klas, M.; Clark, E.; McManus, J. Origin of the northern Atlantic’s Heinrich events. *Clim. Dyn.* **1992**, *6*, 265–273. [[CrossRef](#)]
45. Moros, M.; Kuijpers, A.; Snowball, I.; Lassen, S.; Backstrom, D.; Gingele, P.; McManus, J. Were glacial iceberg surges in the North Atlantic triggered by climatic warming? *Mar. Geol.* **2002**, *192*, 393–417. [[CrossRef](#)]
46. Erbs-Hansen, D.R.; Knudsen, K.L.; Olsen, J.; Lykke-Andersen, H.; Underbjerg, J.A.; Sha, L. Paleooceanographical development of Sisimiut, West Greenland, during the mid- and late Holocene: A multiproxy study. *Mar. Micropaleontol.* **2013**, *102*, 79–97. [[CrossRef](#)]
47. Govin, A.; Holzwarth, U.; Heslop, D.; Keeling, L.F.; Zabel, M.; Collins, J.A.; Chiessi, C.M. Distribution of major element in Atlantic surface sediments (36° N–49° S): Imprint of terrigenous input and continental weathering. *Geochem. Geophys. Geosyst.* **2012**, *13*, Q01013. [[CrossRef](#)]
48. Demina, L.L.; Galkin, S.V. Factors Controlling the Trace Metal Distribution in Hydrothermal Vent Organisms. In *Trace Metal Biogeochemistry and Ecology of Deep-Sea Hydrothermal Vent Systems*; Handbook of Environmental Chemistry; Demina, L.L., Galkin, S.V., Eds.; Springer International Publishing AG: Basel, Switzerland, 2016; Volume 50, pp. 123–142.
49. Demina, L.L.; Oskina, N.S.; Gablina, I.F. Elemental composition of the foraminiferal tests in the Atlantic Ocean. In Proceedings of the 6th International Conference “Environmental Micropaleontology, Microbiology and Meiobenthology, Moscow, Russia, 19–22 September 2011.
50. Demina, L.L.; Oskina, N.S. New data on the trace metal composition of the planktonic foraminifera microfossils of the Atlantic Ocean. *Doklady Earth Sci.* **2016**, *471*, 1193–1198. [[CrossRef](#)]
51. Demina, L.L.; Galkin, S.V. Ecology of the bottom fauna and bioaccumulation of trace metals along the Lena River–Laptev Sea transect. *Environ. Earth Sci.* **2018**, *77*, 43–55. [[CrossRef](#)]
52. Brummer, G.J.A.; van Eijden, A.J.M. “Blue-ocean” paleoproductivity estimates from pelagic carbonate mass accumulation rates. *Mar. Micropaleontol.* **1992**, *19*, 99–117. [[CrossRef](#)]
53. Budko, D.F.; Demina, L.L.; Novichkova, E.A.; Polyakova, Y.I.; Kravchishina, M.D.; Melenevsky, V.N. Postglacial sedimentation in the White Sea (Northwest Russia) reconstructed by integrated microfossils’ and geochemical data. *Quat. Res.* **2019**, in press.
54. Lea, D.W.; Mashiotta, T.A.; Papenfuss, T.; Martin, P.A.; Sarnthein, M. Variation of foraminiferal Sr/Ca over Quaternary glacial-interglacial cycles: Evidence for changes in mean ocean Sr/Ca? *Geochem. Geophys. Geosyst.* **1999**, *1*, 1004.
55. Stoll, H.M.; Schrag, D.P. Are seawater Sr/Ca variations preserved in Quaternary foraminifera? *Geochim. Cosmochim. Acta* **1999**, *63*, 3535–3547. [[CrossRef](#)]
56. Elderfield, H.; Ganssen, G. Past temperature and  $\delta^{18}\text{O}$  of surface ocean waters inferred from foraminiferal Mg/Ca ratios. *Nature* **2000**, *405*, 442–445. [[CrossRef](#)]

